Laterally Bound Co-porphyrin on CdTe QD: a Long-Lived Charge-Separated Nanocomposite

Jayanta Dana,*,† Ramsha Khan,† Timo Weckman,‡ Karoliina Honkala,‡ and Nikolai V. Tkachenko*,†

†*Chemistry and Advanced Materials Group, Faculty of Engineering and Natural Sciences, Tampere University, 33720 Tampere, Finland*

‡*Department of Chemistry, Nanoscience Center, University of Jyväskylä, 40014 Jyväskylä, Finland*

E-mail: jayanta.dana@tuni.fi; nikolai.tkachenko@tuni.fi

Abstract

Cobalt porphyrin (CoP) derivatives are potential compounds for photocatalytic CO_2 reduction which must be activated by photoinduced electron transfer from a suitable electron donor. Herein, we have prepared and studied the photophysics of CdTe quantum dots (CQD) coupled with CoP derivative where CQDs act as the light antenna and the electron donor and CoP act as the electron acceptor. To facilitate the nanocomposite formation of CoP with CQD, CoP has been equipped with a −COOH anchoring group which leads to strong complexation between CQD and CoP as observed in the absorption spectra by a gradual shift in the Soret absorption band. This is attributed to the lateral binding geometry of CoP through the −COOH anchoring group and Co-center coordination to CQD, which helps to bring CoP close to the CQD. Our DFT calculations have identified that this lateral geometry is more favorable than the upright orientation on the CdTe (110) surface. The redox levels have been determined from cyclic voltammetry which show that the electron transfer (ET) from CQD

to CoP is feasible. The strong luminescence quenching of CQD in the presence of CoP has also suggested quantitative CQD/CoP nanocomposite formation and pointed to the ET from QDs to CoP. The charge carrier dynamics have been monitored using femtosecond transient absorption (TA) spectroscopy. The TA spectral analysis have shown efficient ET in CQD/CoP which proves that our 4 nm CQD acts as an efficient electron donor for the CoP counterpart. The CQD excited state lifetime is shortened along with delayed Soret band bleaching of CoP in this nanocomposite. From the global fitting of TA data, the estimated average ET time constant from CQD to a CoP molecule is approx. 70 ps and the charge recombination time is $\gg$5 ns. Also, differences in the TA spectra after ET have been observed which can be associated with the changes in the binding geometry of CoP on CQD surface, that is lateral in case of ground state complex to the upright orientation after the ET process. Hence, the studied CQD/CoP nanocomposites are promising materials to initiate CO_2 reduction through photoexcitation of the CQD that activates the CoP molecular catalyst through the ET.

Introduction

The rapid increase in atmospheric CO_2 [1] has driven research towards CO_2 capture and storage technologies.[2] Converting the stored CO_2 into fuels and other value-added compounds is an important but challenging task as CO_2 is thermodynamically very stable and the conversion process requires additional energy. The general approach to CO_2 reduction is to use a suitable catalyst which is activated by an electron transfer (ET) from a source with sufficiently high potential energy.[3,4] The first-row transition metals, such as Fe and Co, are used as molecular catalysts in both electro- and photocatalytic applications where they are part of the organic frameworks such as porphyrins.[5–7] In particular, metal porphyrin (MP) derivatives have shown promising results in electrocatalytic and photocatalytic CO_2 reduction.[4,5,7,8] Photocatalytic CO_2 conversion is an advanced approach, whereby the reaction is driven by

solar energy. Photocatalytic applications make use of photo-induced electron transfer (PET) to deliver electrons to a catalytic center. Therefore, the catalyst, e.g. MP, must be coupled with a suitable electron donor which absorbs a photon and the electron transfer (ET) takes place from its excited state to the catalyst.

Coupling MP with semiconductor quantum dots (QDs) is a promising approach to initiate the CO_2 reduction through the PET from QD to MP.[7,9,10] Due to extraordinary photophysical properties of QDs, such as easily tunable band gap, high extinction coefficient in the visible range, multiple excitons generation, and easy surface modification,[11–17] the QDs are ideal candidates for solar energy devices. The QDs serve both as a light antennas and an electron donors while the MP operates as a molecular catalyst activated through the PET between the former and the latter as outlined in Figure 1.[10] If the lowest unoccupied molecular orbital (LUMO) of MP attached to QD is lower in energy than the lowest edge of the QD conduction band (CB), the electron can be transferred from the QD to MP in a PET reaction.[18–20] The advantage of MP-QD nanocomposite materials is the long lifetime of a charge-separated state, which is essential for photocatalytic and solar cell applications.[7,19,21] In particular, the QD-MP nanocomposite system can efficiently and selectively reduce CO_2 to CO.[7,9] Recently, Arcudi et al. reported 98 % efficiency of CO_2 reduction with 99 % selectivity for CO production using $CuInS_3$ QDs - Co-porphyrin nanocomposites.[7]

Ultrafast transient absorption (TA) spectroscopy is a classic technique to probe the charge transfer and recombination dynamics in solar energy devices. The TA response of QDs allows to monitor the photo-induced carrier cooling, state filling, and carrier recombination.[22–24] When a QD absorbs a photon with energy larger than its band gap, a hot exciton is generated and it relaxes quickly to its band edge releasing excess energy in a process called carrier cooling.[25] After this cooling, the carrier fills the lowest available band edge (BE) level depending on the band degeneracy. In II-VI QDs, the CB and the valence band (VB) are 2 and 4-fold degenerated, respectively.[18,23,26] In TA spectroscopy, the filling of the CB by electrons is observed as bleaching in the wavelength range corresponding to the BE.[23,26,27]

The ultrafast charge transfer dynamics of II-VI QDs and molecular adsorbates have been studied extensively.[18,28–30] The ET process is typically investigated by monitoring the change of the QD lifetime and anion formation of a molecular adsorbate.[20,28] In general, the ET time from II-VI QDs to a molecular adsorbate is found to be from sub-picoseconds to some hundreds of picoseconds depending on the types of QDs and molecular adsorbate.[28,29]

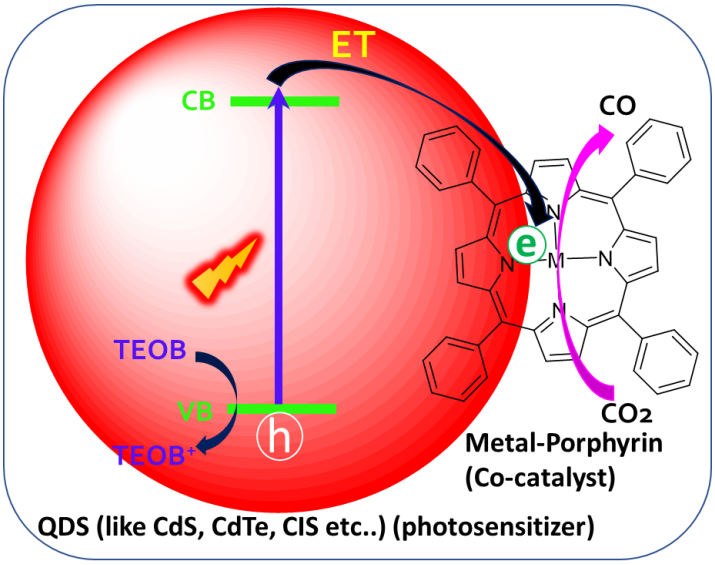

Figure 1: Schematic presentation of photo-initiated CO_2 reduction by QD-MP nanocomposite.

The MPs have narrow Soret bands along with a few broad Q bands[31,32] which can be used to monitor the state of MP in PET reactions in CQD/MP nanocomposite via TA techniques. Mandal et al. reported a hot ET from CdTe QDs to tetrakis(4-carboxyphenyl)porphyrin (TCPP).[29] On the other hand, Aly et al. explored the ET from meso-tetra(N-methyl-4-pyridyl)porphine tetrachloride (TMPyP) to QDs.[33] Weiss group has shown the reduction of CO_2 using $CuInS_2$/ZnS core/shell QD and iron porphyrin nanocomposites.[34] The proposed photocatalytic CO_2 reduction mechanism starts with the activation of the iron porphyrin catalyst through the PET from a photo-exited QD.

Despite successful demonstrations of CO_2 reduction by QD-MP, many questions on the mechanism and efficiency of the PET and the effect of QD and MP mutual orientation in these systems remain unanswered. Also, the back electron transfer (BET) is a critical

parameter, and the sufficiently long lifetime of the charge-separated (CS) state (or a slow BET) is an important prerequisite to achieve efficient catalytic reactions which are relatively slow diffusion-controlled processes.

In order to address these issues, we selected 4 nm CdTe QDs (CQD) and cobalt tetraphenylporphyrin derivative (CoP) equipped with $-$COOH anchoring group, and employed the ultrafast TA spectroscopy to characterize the PET reaction quantitatively in this nanocomposite. The advantage of the selected CQD is a broad absorption of CQD covering the whole visible spectrum. In addition, this CQD-CoP combination is characterized by favorable thermodynamics for PET leading to the formation of $(CoP)^-$ which is known to be a suitable catalystic state for CO_2 reduction.[35] The steady-state absorption spectra show the formation of a new band at 465 nm, which is due to the shifted Soret band of the CoP molecule and points to a complexation between CoP and CQD. We propose that the CoP molecule binds to the CQD surface in a lateral orientation having additional coordination between CQD and Co metal. We find this geometry favorable in the density functional theory (DFT) calculations. The complex formation is also confirmed by a strong luminescence quenching of CQD in presence of CoP. Femtosecond TA spectroscopy has been employed to confirm the electron transfer in CQD/CoP nanocomposite systems. From the global fitting of TA data, the measured ET time constant from CQD to per CoP molecule is $\approx$72 ps and the charge recombination time is $\gg$5 ns or longer than the available delay time from the used instrument. Therefore, we found a long-lived CS state between CQD and CoP which makes it a promising nanocomposite for CO_2 reduction.

Experimental Section

Synthesis of CdTe QDs

Oleic acid (OA) capped CQDs were synthesized following reported procedures.[36] 1 mmol CdO, 4 mmol OA and 20 mL of octadecene (ODE) were taken together in a 100 mL three

neck round bottom flask. We purged it with Ar gas for 1 hour at 130 °C and then heated it to 280 °C to dissolve CdO completely. The formation of colourless solution presents the formation of Cd-Oleate. In another reaction mixture, we have prepared Se-precursor separately by dissolving 0.5 mmol Se powder in 1 mL trioctylphosphine (TOP) and 2 mL ODE. The Se-precursor was injected into Cd-precursor at 280 °C with Ar flow and left for a few minutes to get the desired size of CQD. Finally, the reaction was quenched in a water bath. After cooling down, the synthesized CQDs were precipitated several times by methanol and dissolved in toluene for further use.

Porphyrin derivatives

The Structure of free base porphyrin (H_2P), cobalt-porphyrin (CoP1) and CoP are shown in Figure 2. The H_2P and CoP1 were purchased from Por-Lab and Sigma-Aldrich, respectively. We prepared the CoP after incorporating Co metal into purchased H_2P following a reported method.[37]

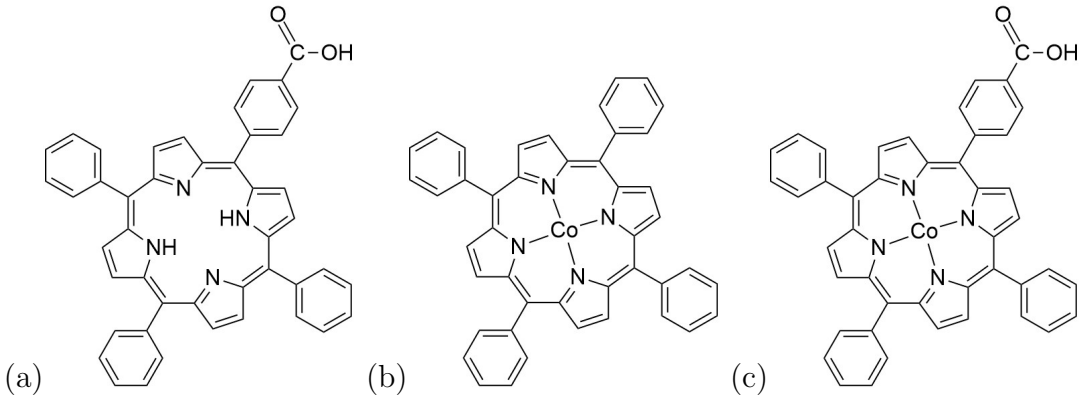

Figure 2: Structures of (a) H_2P , (b) CoP1 and (c) CoP

Femtosecond transient absorption spectroscopy

All the TA measurements have been carried out in toluene using a 2 mm cuvette. The 800 nm laser pulses with 1 mJ energy were generated by Libra F (Coherent Inc.) and split into two arms. The first one generated white light continuum (400–800 nm) after focusing 800 nm

pulses on a water cuvette and another one was passed to Topas OPA (Light Conversion Ltd.) to generate tunable pump. Two wavelengths, 610 and 680 nm, were used as excitation wavelenghts (pump). Exci-Pro spectrometer (CDP Inc.) equipped with a CCD array for the visible spectral range (400–750 nm) was used to measure TA spectra (probe) in delay up to 6 ns. The used pump intensity was sufficiently low to avoid multiple excitons generation.

Computational details: The CoP adsorption on the (110) surface was studied using DFT calculations as implemented in the GPAW[38] software. The exchange–correlation part of the total energy was approximated using the Perdew–Burke–Ernzerhof (PBE)[39] exchange–correlation functional together with the Hubbard-U correction. The U values were set at 5.0 and 3.0 eV for the valence *d*-electrons of Co and Cd atoms, respectively, and at 2.0 eV for the valence *p*-electrons of Te. The weak dispersion interaction was treated using the dispersion correction proposed by Grimme and co-workers.[40] The Kohn–Sham equations were solved using a plane-wave basis set with a cutoff energy of 500 eV. The reciprocal space was sampled using $6 \times 6 \times 6$ Monkhorst–Pack mesh for the CdTe primitive cell and $3 \times 3 \times 1$ and $3 \times 2 \times 1$ k-point meshes were used for the 3×2 and 3×4 (110) surface cells, respectively. The atomic structure optimization was finished when the residual forces were below 0.05 eV/Å on each atom. Further computational details can be found in the Supporting Information.

Results and Discussions

Steady state absorption and emission spectroscopy

Figure 3 shows the absorbance and emission spectra of synthesized CQD. The absorbance spectrum has a distinct energy level structured due to quantum confinement. The band edge (BE) ($1S_e$–$1S_h$ transition) (1S) and above BE transitions ($1P_e$–$1P_h$ transition) (1P) are at 662 and 565 nm, respectively. The first absorbance peak corresponds to the 4 nm diameter of CQD.[41]

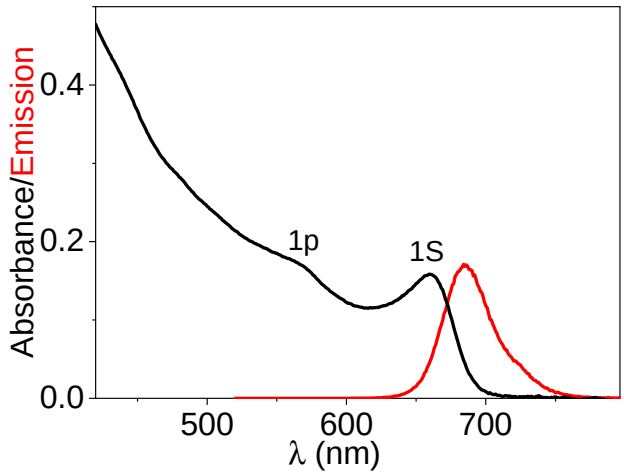

Figure 3: Absorbance (black) and emission (red) spectra of QDs.

To test the photophysical interaction between CQD and CoP molecules, the steady state absorbance and emission spectroscopy measurements were carried out. Figure 4 (left panel) shows the change of absorbance of CQD on the addition of CoP molecules in toluene solvent. The concentration of CQD was fixed but six different concentrations of CoP were used: 1.23, 2.47, 3.71, 4.95, 6.6, and 9.9 μM. The luminescence quenching of CQD increases with the increasing number of CoP attached to it, as presented in Figure 4 (right panel). The luminescence of CQD is quenched 94 % at the used highest concentration of CoP. To calculate the exact ratio of the concentrations of [CQD] and [CoP], the relative emission of the CQD, I/I_0 (where I_0 and I are the emission intensities of CQD in the absence and presence of CoP, respectively) has been plotted as a function of the CoP concentration, as shown in Figure 4 (right panel), and fitted assuming statistical complex formation with the Poisson distribution of the number of CoP attached to a CQD and complete emission quenching of CQD if at least one CoP is attached to CQD.[42] Thus calculated concentration of CQD is in reasonably good agreement with the concentration estimated based on the reported molar absorption coefficient of CQD with an absorption maximum at 660 nm.[43] As a reference, a 94 % quenching is achieved at ratio of [CQD]:[CoP]=1:3, which corresponds to [CQD] = 3.3 μM at highest [CoP] = 9.9 μM in our case (Figure 4, right panel).

The 1S and 1P bands of CQD are not changed at all in the presence of the CoP molecule

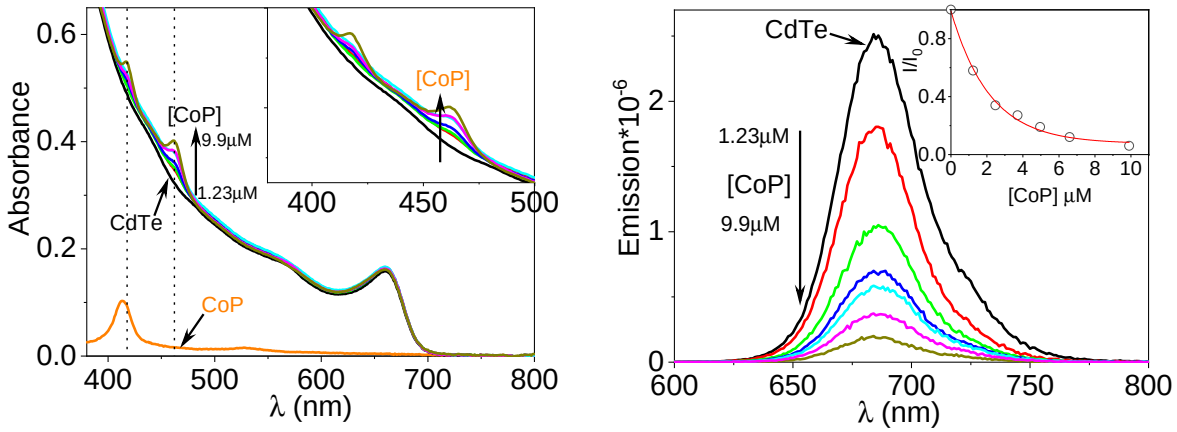

Figure 4: Left Panel: Absorbance spectra of CoP, CQD and CQD in presence of 1.23, 2.47, 3.71, 4.95, 6.6 and 9.9 μM CoP in toluene solvent. Right Panel: Luminescence spectra of CQD and CQD/CoP same composition corresponding to absorbance spectra. Inset: Plot of I/I_0 vs. CoP concentration.

(Figure 4, left panel, in the range 600–700 nm), pointing to the unchanged ground state of CQD. On the other hand, the absorbance spectrum of CoP does change in the presence of CQD. The absorbance spectrum of CoP in toluene is shown in Figure 4, left panel and is characterized by a narrow band at 415 nm (Soret band) due to S_0-S_2 transition and broad and poorly resolved two bands in the 530–600 nm range corresponding to S_0-S_1 transition (Q bands).[44] Absorbance spectra of the CQD/CoP mixture show that a new band develops at 465 nm and the strength of original Soret band decreases. The new band at 465 nm is not a new transition, but it is a 50 nm red-shifted Soret band in presence of CQD surface. Along with the Soret band, the Q bands are also red-shifted, indicating a complex formation between CQD and CoP. This large shift of absorption is very unusual for metal-porphyrin, and is typically caused by a deformation of the planar porphyrin skeleton in the event of complexation. Haddad et al. explained the reason behind the large shifting of absorbance band by deformation of the metal-porphyrin framework.[44] They have reported the shift for Soret and Q bands similar to those that we have observed.

To find the reason behind the Soret band shift, two test experiments were carried out: (1) CoP was mixed with trioctylphosphine-telluride (Te-TOP), and (2) Co-porphyrin without −COOH group (CoP1, see Figure 2) was mixed with CQD. Figure S2 in ESI compares

spectra perturbations in CoP/CQD and CoP/Te-TOP samples. The same 50 nm shift of the Soret band and a similar shift of the Q bands are observed in both cases of mixing CoP with CQD and Te-TOP, proving the interaction between Te and CoP. However, when CoP1 is mixed with CQD, no perturbation of absorbance spectra of CoP1 is observed (see ESI Figure S3), and no emission quenching of CQD is seen as well, demonstrating that without carboxylic anchor no complexes were formed. Figure S4 shows the comparison of Soret band absorbance in CQD/CoP, CQD/CoP1, CQD/H_2P, and Te-TOP/CoP. It's clearly visible that Soret band shiftings are exactly the same for both CQD/CoP and TeToP/CoP cases. Therefore, the 50 nm shifting of CoP absorbance was only observed when CoP had an anchoring group along with the metal center. Considering all this evidence, we assume that CoP interacts with CQD at two sites, one is the $-$COOH group binding to the CQD surface and another is the co-ordinate of Co to the Te site in CQD. This results in a kind of "two points" binding with CoP "lateral" orientation in respect to the CQD surface.

The two points interaction between CQD and CoP and especially co-ordination of Co, creates a strain on the CoP frame, resulting in the deformation of the CoP core and a large red shift in the absorption. The special lateral binding geometry helps the CoP to come close to the surface of CQD. From time-dependent DFT calculation Hege et. al.[45] proposed explanation of the effect of nonplanar distortions on the electronic spectrum shift to the red. The metal(d)-porphyrin (π) orbital interaction is symmetrically forbidden in the planner metal-porphyrin, but it switches to symmetrically allowed to some extent on the event of a distortion, resulting in absorption spectra red-shifts largely. Not only metal(d)-porphyrin(π) orbital interaction, metal(d_{xy})- porphyrin(a_{2u}) antibonding interaction has also a significant role in this redox level. On ruffling of the porphyrin ring the metal(d_{xy})-porphyrin(a_{2u}) becomes symmetry-allowed, resulting in raising the orbital energy of the HOMO.

At experimental conditions, most of the CoP has this "two points" coordination. However, in addition to the shifted Soret band, a smaller band can be found at the traditional non-disturbed Soret band position, depicting the presence of some amount of CoP without

Co coordination to CQD. The proportion of CoP with "normal" Soret band to that with shifted band increases when the ratio [CoP]:[CQD] increases over 5:1. A detailed study of the proportion between CoP and CQD for the different coordination modes is discussed in ESI, Figure S5. The highest ratio of CoP and CQD used herein is 3:1 for a detailed study.

CoP binding onto the CdTe surface

The binding modes of the CoP molecule on the CdTe quantum dot were examined using the non-polar, low-index zinc-blende surface (110), which corresponds to the lowest surface energy structure for a similar cadmium chalcogenide material, CdS.[46]

We considered two CoP orientations on the surface: an upright and a lateral geometry, please see Figure 5. In the upright geometry, we screened several binding sites and the CoP molecule prefers to bind to the Cd atoms of (110) via the carboxylic anchor group in a bidentate fashion (see Figure 5. The molecular axis of the CoP is tilted by approximately 30 degrees with respect to the surface plane. This bending is more stable than a fully upright by -0.27 eV. The distance between the oxygen atoms in the carboxylic group and the surface Cd atoms are 2.30 and 2.35 Å in the optimal geometry. For comparison, the Cd−Te bond distance in the bulk is 2.78 Å.

The lateral binding mode was constructed from the upright geometry by bending the porphyrin ring towards the surface so that the ring lies parallel on the surface. Different orientations for the CoP were considered. In the optimal configuration, the carboxylic group remains bonded with the surface Cd-atoms and the cobalt atom in the porphyrin ring is able to bind with a surface Te-atom. The Co–Te coordination results in a significant distortion of the porphyrin ring as depicted in Figure 5. The Co–Te bond length is 2.99 Å and the Cd–O distances are 2.24 and 2.27 Å.

Energetically the lateral binding mode is significantly more stable than the upright one. The binding energy of CoP in the slightly bended upright orientation is −3.57, while the binding energy for the lateral orientation is −4.41. Thus, the lateral geometry results in

a further stabilization of −0.84 over the upright geometry. The computationally identified distortion of the molecular ring can help to explain the experimentally observed shifts in the Soret and Q bands discussed above.

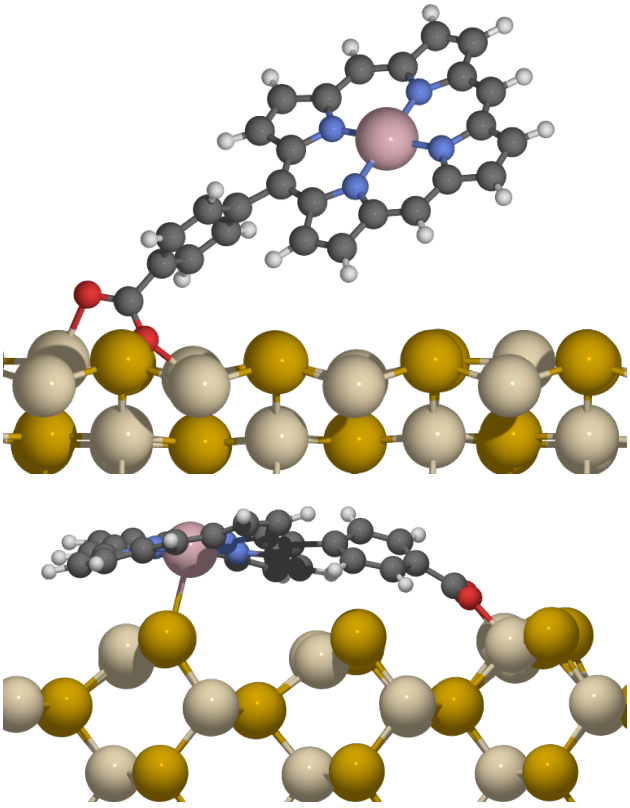

Figure 5: CoP molecule adsorbed onto the (110) surface in an upright (top) and a lateral orientation (bottom).

Under experimental conditions, the surface of the colloidal quantum dot is capped by ligands, for example oleic acids. The binding of these ligands competes with the binding of the CoP. We mimic the oleic acids with carboxylic acid with different carbon chain lengths (please see SI for more information). Our results show that in general the binding energies of the CoP molecule are more exothermic than the binding energies of considered carboxylic acids. While in the upright binding mode, the surface area adopted by the CoP is roughly equal to one carboxylic acid ligand molecule, in the lateral binding mode, the CoP needs more space, which could, in turn, require the removal of some ligand molecules from the surface of the quantum dot. However, the energy gain from the CoP adopting the lateral

binding mode over the upright one is smaller than the binding energy of a carboxylic acid ligand molecule making the exchange process thermodynamically unfavourable.

From steady-state absorption, emission, and DFT calculation, We have found a lateral binding geometry between CQD and CoP, where the emission of CQD is quenched. The possible mechanisms behind the luminescence quenching of CQD in presence of CoP can be either electron transfer or energy transfer or both electron and energy transfer from CQD to CoP.[30,47–49] The energy transfer is not a favorable process in this nanocomposite as there is no overlap between the luminescence spectra of the donor (CQD) and the absorption spectra of the acceptor (CoP).

The thermodynamic feasibility of the ET can be deduced from the energy comparison of the CB bottom of CQD and the LUMO of CoP. We used differential pulse voltammetry (DPV) to calculate the redox levels of CoP and CQD, as shown in Figure S7. The energies of interest are the LUMO of CoP and the CB bottom of CQD, which are at -3.27 eV and -3.76 eV, respectively. This clearly shows that PET is possible and it has a relatively large driving force of 0.5 eV.

Femtosecond TA studies

In order to confirm the ET from CQD to CoP molecule and to evaluate ET and BET rate constants, we have employed femtosecond TA spectroscopy. Figure 6a shows the TA spectra of CQD at different delay times in the range from 0.75 ps to 5 ns following 600 nm excitation pulse. The fastest process, around 1 ps, can be attributed to carrier cooling and the longest to the final electron-hole pair recombination. We can see the distinct bands corresponding to different transitions in CQD spectra, a dominating 1S and a minor 1P transitions are at 665 and 567 nm, respectively. In addition to these bands, another bleach for higher transition at 450 nm is observed. We used sufficiently low excitation density ($\approx$5 % of saturation) to generate predominantly the single exciton excited state and avoid multiple exciton generation.

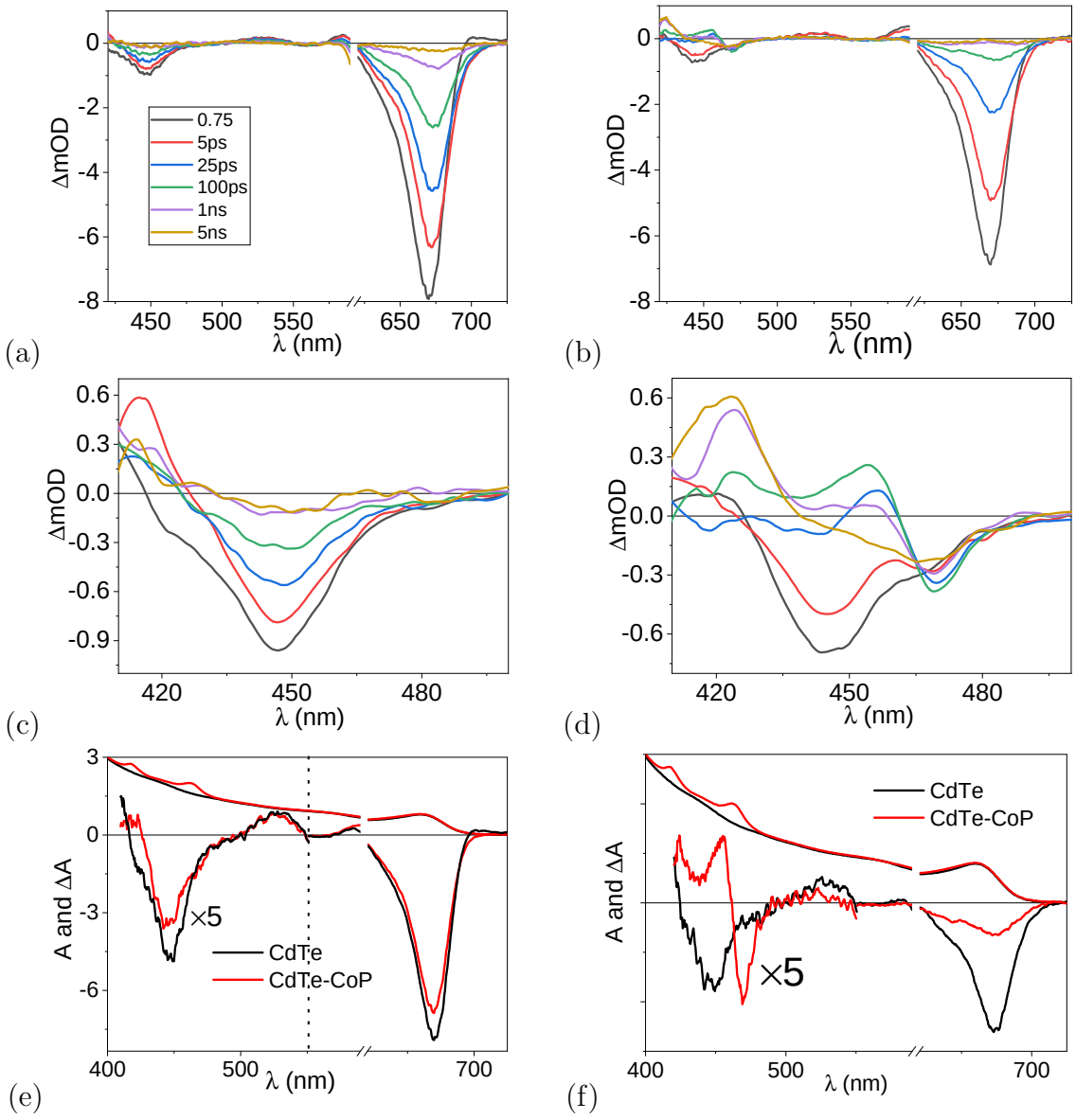

Figure 6: TA spectra of CQD (a) and CQD/CoP (b) following 600 nm excitation in toluene. (c) and (d) are the same spectra as in (a) and (b) but expanded in the 410–500 nm range. Ground state absorbance (normalized) and difference spectra for CQD and CQD/CoP at 0.75 ps (e) and 100 ps (f) time delay.

The similar TA spectra of CQD/CoP nanocomposite with 94 % emission quenching (corresponding to [CoP]:[CQD]≈3:1) are presented in Figure 6b. The TA measurements of CQD and CQD/CoP nanocomposite were carried out in the same condition with the same pump fluency, and the excitation pump fluency must be roughly the same in both cases. The spectral shape at the BE (1S) of CQD/CoP sample is the same as that of CQD, though the bleach recovery is much faster in the case of CQD/CoP sample. In addition, there is an important difference between two samples in the range 420–550 nm starting from a few ps delay as shown in Figures 6c and d.

At a very early delay time (at 0.75 ps), the spectra for CQD and CQD/CoP nanocomposite are the same (Figure 6e), but with time a new band develops with a maximum close to 467 nm. At 100 ps delay, a completely distinguished band at 467 nm is observed (Figure 6f). The ground state absorption of the sample and TA spectra at 0.75 and 100 ps are compared in Figures 6e and 6f, respectively, and one can see that a new band develops at the same position as the Soret (shifted) band. It indicates that CoP gets involved in the excitation relaxation of the CQD/CoP complexes at tens of ps delay time.

The pump at 600 nm excites predominantly CQD since at this wavelength, the absorbance of CoP is very negligible compared to that of the CQD. Nevertheless, the TA response of CoP alone was tested separately and the results are presented in ESI Figure S7. The Soret band at 420 nm is instantly bleached after excitation, but the lifetime of the excited state is very short (few ps) in agreement with the previous reports.[50,51] The TA response of CQD/CoP complexes is different, especially the time scale of the response is much longer compared to that of pure CoP solution.

Another distinct feature of the TA response of CQD/CoP complexes is that while the bleaching of the CoP Soret band shapes up, the features of the CQD excited state disappear. This can be seen from both the bands at 670 and 445 nm. For example, at 100 ps the bleaching at 670 nm, the CQD band edge region, is almost recovered but the CoP Soret band bleaching is close to its maximum. The energy transfer from CQD to CoP can be

excluded since the excited state energy of CQD is lower than that of CoP as was discussed above. Another reason to exclude the energy transfer is that the lifetime of the CoP excited state is short, a few tens of ps at maximum, but the response of CoP in CQD/CoP complexes is well observed at a few nanosecond delay times. However, the observed behavior is in line with the electron transfer from CQD to CoP.

An excited CQD has one electron at the bottom of CB which leads to the bleaching at the band edge wavelength. The ET removes the electron from the CB and results in an almost complete recovery of the absorption at 670 nm.[18,52] At the same time, an extra electron at CoP changes the absorption of the porphyrin which is observed as the bleaching of the strongest absorption band, the Soret band. This extra electron at CoP side cannot relax within CoP molecule, and must recombine with the hole left in the CQD. This must be a slow process leading to a long-lived intermediate in TA measurements.

The TA data were fitted globally (see ESI for details) to identify and quantify the intermediate states formed during the excited state relaxation including carrier cooling, carrier trapping, ET from CQD to CoP, and BET from CoP to CQD. The decay-associated spectra (DAS) obtained by the global fit of CQD and CQD-CoP samples are shown in Figures 7a and 7b, respectively. CQD TA data were fitted by a combination of exponential ("Exp1") and Poisson ("Pois") decay functions (see ESI for details). The former model represents carrier cooling down to the bottom of the CB, and the latter is designed to model the decay of CQD with possible defects having Poisson distribution.[20] The estimated cooling time, 0.45 ps, is in good agreement with previously reported results.[25,53]

The second component, the Poisson decay function, depends on three parameters, the relative quencher (trap state) concentration, c_t, trapping time constant, τ_t, and the excited state lifetime of the trap-free CQD, τ_0. The calculated parameters are $c_t = 1.2$, $\tau_t = 70$ ps, and $\tau_0 \approx 2.5$ ns, respectively. The value of τ_0 is much shorter than the emission decay measured using the time-correlated single photon counting method which is due to a limited time scale available from the pump-probe instrument, roughly 5 ns. However,

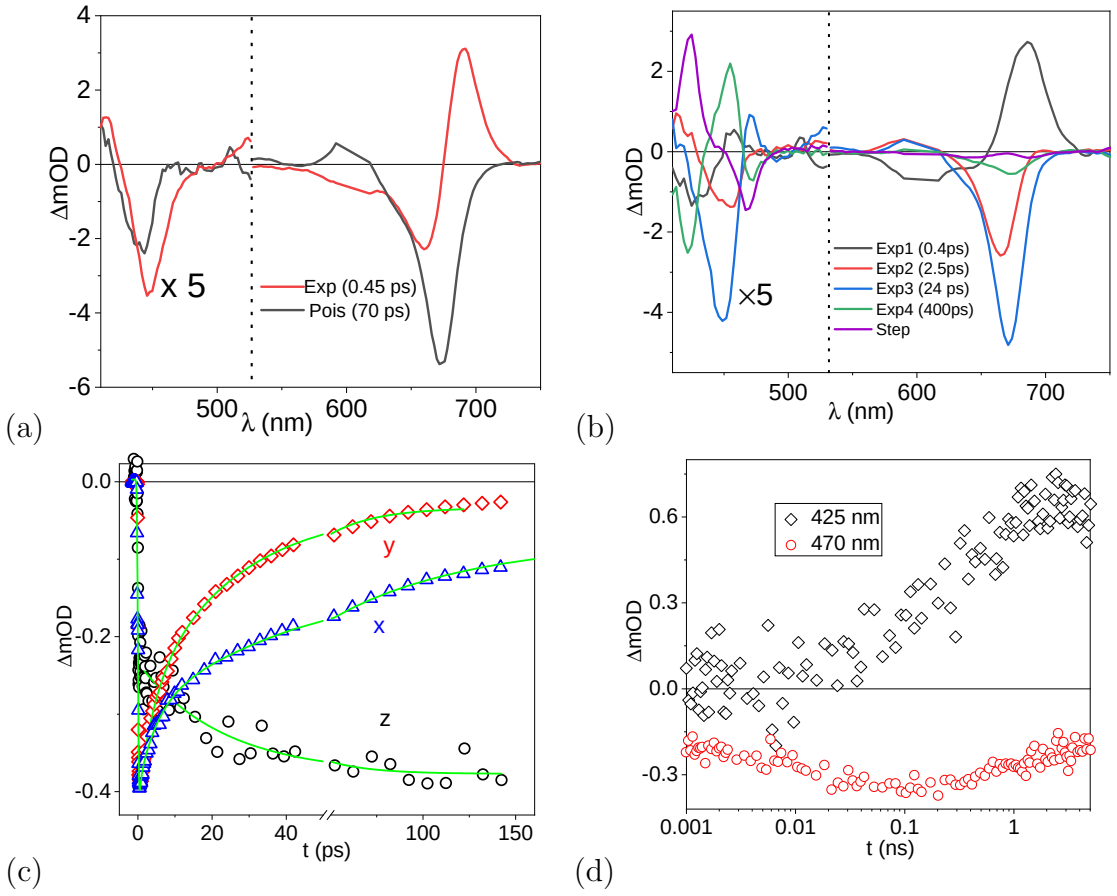

Figure 7: Fitted decay associated spectra (DAS) of CQD (a) and CQD/CoP nanocomposite materials (b) following 600 nm excitation in toluene (from figure 6). (c) Spectral cuts of CQD (x) and CQD/CoP (y) at the BE (670 nm) and the Soret band (467 nm) for CQD/CoP nanocomposite (z). (d) Spectral cuts of CQD/CoP at 470 nm and 425 nm.

the other two values are reasonable and consistent. In particular, the fit suggests that the emission quantum yield of QDs is not greater than $e^{-c_t} = 0.3$, which agrees with steady-state measurements (0.18).

The CQD-CoP TA data were fitted using a sum of four exponents ("Exp1", "Exp2", "Exp3" and "Exp4" in Figure 7b) plus a step function ("Step") which represents a long-lived state without detectable decay within the instrument time scale, 5 ns. The fastest component, 0.4 ps, is similar to that of the CQD sample and can be attributed to carrier cooling. The following process, 2.5 ps, results in a minor recovery of the beaching associated with CQD excited state and it is not clear what is the origin of this relaxation. However, the dominating component in terms of the bleaching recovery has a time constant of 24 ps, and in addition to the bleaching it has a positive band close to 470 nm, which is the absorption wavelength of CoP. This component indicates that while the excited CQD population decays, the ground state of CoP molecules is depopulated, or CoPs are promoted to another state. As discussed above the most feasible interpretation is the electron transfer from the excited state of CQD* to CoP, or $\mathrm{CQD} + h\nu \longrightarrow \mathrm{CQD}^*$ and then $\mathrm{CQD}^* + \mathrm{CoP} \longrightarrow \mathrm{CQD}^+ + \mathrm{CoP}^-$. The 24 ps time constant is an "observable" lifetime, but since on average each CQD should have three CoP attached to it, the estimated ET time constant in an "ideal" one-to-one complex is roughly 72 ps.

The ET reaction is not the last one in the measured time window. The reaction with 400 ps time constant has a very minor signal at the BE wavelengths (600–700 nm) but a strong response in the blue part of the spectrum (400–500 nm). The reaction results in a very long-lived ($\gg$10 ns) state with the differential spectrum presented by the "Step" component attributed to a very long-lived charge-separated state. The distinct features of this state are still bleached 470 nm band and increased absorption at 420 nm, which corresponds to non-coordinated CoP.

To visualize the ET more clearly, we present spectral cuts of CQD (x) and CQD/CoP (y) nanocomposite at the BE (670 nm) and shifted Soret band position at 470 nm (z)

in Figure 7c. At the BE, one can follow the depopulation of the excited state of CQD which is faster for CQD with CoP than without CoP. Then, taking into account the band structure of this II-VI semiconductor, we can see that the CB and VB are two- and four-fold degenerate, respectively, and the hole (h) is heavier than the electron (e).[18,23,25] The e and h contributions to the TA bleach of this type of QDs is still under debate.[24,26] So far, no hole contribution was observed in the TA bleach for nascent CdSe or CdTe QDs. The e at the CB is mainly responsible for TA bleach. Therefore, if the e transfers from the CB of QDs to any other state or location, there is no more blocking of the transition corresponding to the BE since the effect of e on the stransition is much smaller effect and the degeneracy of hole at VB is higher. As a result, the bleach dynamic follows the e state and decays with ET. Simultaneously, the development of bleach at 470 nm with the same rate as the depopulation of the CQD excited state can be attributed to the ET from CQD to CoP. To explain what is happening after ET or where e can be localized, one may follow the spectral cuts at 420 and 475 nm in Figure 7d. During the growth of the bleach at 470 nm arising from the ET, the absorbance at the 420 nm is negligible. It means that the absorbance rising at 420 nm is delayed by a few hundreds of ps and it starts to grow after the ET. The absorbance rises at 420 nm coincides with a small recovery at 470 nm. The CoP^{-} is generated after the ET from the excited CQD. It can be discussed if the e is first localized at the porphyrin π-conjugated ring and then is transferred to Co changing its state from Co^{II} to Co^{I}, or it is directly transferred to Co avoiding localization at the porphyrin ring. In any case, the electron transfers from the porphyrin ring to Co (or $Co^{II}(P^{-}) \longrightarrow Co^{I}P$) is the fast and favorable process for metal to ligand charge transfer, and it must take place in a few ps timescales,[50,51] or faster than the ET from the excited CQD, and thus is not experimentally observable in our case. But the change in the Co coordination state affects Co binding to CQD, and we attribute the 400 ps to the loss of Co–CQD coordination, losing lateral binding geometry of the porphyrin ring and thus returns to its Soret band maximum to 420 nm as the result. After the BET the system returns to its initial state. On the other hand, to check

the influence of a trace amount of atmospheric CO_2 and O_2 dissolved in toluene solvent, we have measured TA of CQD/CoP composite in similar conditions after nitrogen purging for a long time to remove dissolved trace amount of CO_2 and oxygen, and compared the results with no purging sample as shown in Figure S8. The spectral shape and kinetics of all the wavelengths are exactly the same. Therefore, we can say that the dissolved atmospheric CO_2 (and oxygen, for that matter) doesn't have any influence on the charge transfer processes in this nanocomposite at least in the time domain shorter than 6 ns.

At 600 nm excitation wavelength, the absorption for CoP is negligible compared to that of CQDs but not zero. Therefore, there is a chance to generate some signal at 467 nm from direct excitation of CoP. To avoid the excitation of CoP completely, the TA experiments were carried out with excitation at 680 nm where absorption for CoP molecule can be completely excluded. The 680 nm pump is at the longer wavelength edge of the 1S band of CQD but completely out of CoP absorption range, as shown in Figure 8a. The downside of the excitation at 680 nm is that the strong pump scattering makes it impossible to monitor the CQD response at BE wavelength range. Therefore, the discussion will be limited to the 400–500 nm monitoring range only.

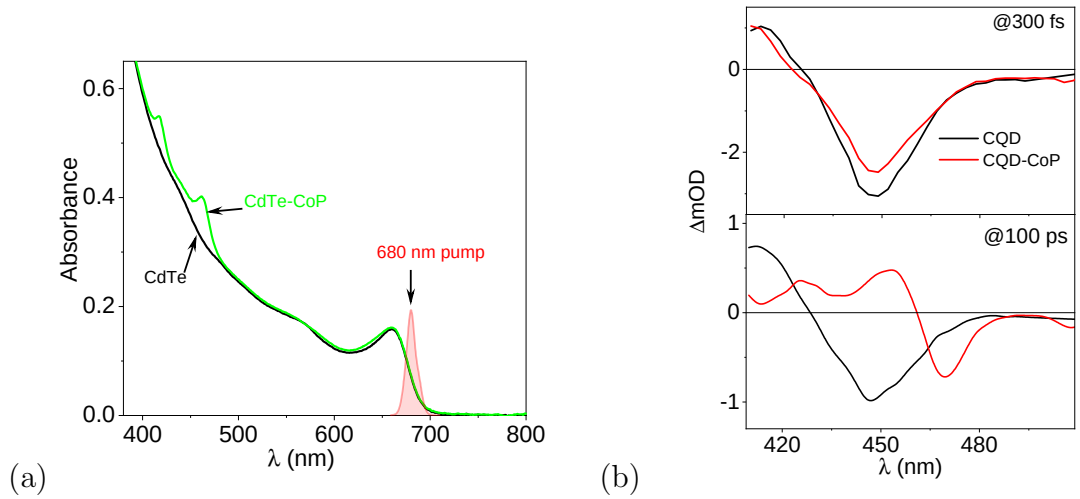

Figure 8: (a) Comparison of overlap between absorption of CQD, CQD/CoP and 680 nm excitation pump spectra. TA spectra of CQD (black) and CQD/CoP red at 300 fs (upper panel) and 100 ps (lower panel) after 680 nm pump excitation in toluene.

Right after the 680 nm excitation, the TA signal is only contributed by the CQD response. Figures S9a and b present the TA spectra of CQD and CQD/CoP nanocomposite following 680 nm excitation. The spectra of CQD in the 410–500 nm range are similar with both excitations at 600 and 680 nm. Also the spectra of CQD/CoP follow the same trend when excited at 600 and 680 nm.

At an early time scale of 300 fs, the spectra of CQD and CQD/CoP are the same, but with time a new band develops at 467 nm in the case of CQD/CoP sample. At 100 ps we can distinguish the separate bleach band at the 467 nm, Figure 8b lower panel. This bleach is very long-lived as well and not decaying within the measurement time window (5 ns) similar to the case of excitation at 600 nm. Figure S7 (C) presents the kinetics of CQD/CoP at 467 nm which is quite similar to that with 600 nm excitation. The TA experiment with 680 nm excitation confirms the ET from CQD to CoP.

There are a few factors which control the electron transfer rate from CQD to CoP and the lifetime of the CS state.

(1) The electronic coupling between the initial (excited) and final (charge transfer) states is the key parameter critical to the electron transfer rate in both forward and back reactions. The electronic wave function of CB of CQD spreads wider as compared to LUMO of CoP because of the larger spherical size of CQD compared to molecular orbital, resulting in relatively slow electron transfer.[54] The CS state is also quite long-lived because of this weak electronic coupling between the donor and acceptor.

(2) The distance between CoP and CQD has a strong influence on the coupling strength between initial (excited) and final (charge separated) states, which can impact both ET and BET. Herein, we didn't study the distance effect on ET and BET, though we expect a very short separation between the CQD and CoP due to the "lateral" binding mode.

(3) Orientation of CoP on the surface of CQD is also an important parameter for ET and BET. It has been already shown that for nanocrystal-molecular acceptor system, the ET is faster in lateral attachment compared to the up-right orientation of the acceptor on

QD surface typical for a through ligand attachement.[55,56] The "lateral" binding mode found here can be considered to provide an optimal geometry for a fast and efficient PET.

(4) The TA data show that the electron-hole recombination is really slow in this CQD/CoP system ($\gg$ 5 ns). The electron and hole decouple quite strongly as the electron is localized at CoP and hole on CQD, which are completely different species. After charge transfer the coordination between CQD and CoP is lost temporarily, and as the result, the electron-hole are separated even more, which slows down the BET rate from CoP^- to CQD^+.

Therefore, we found an unprecedentedly strong complexation between metal-porphyrin and CQD, and a long-lived CS state in a single architecture which can be promising for CO_2 reduction. To prove this, further photocatalysis studies are required.

Conclusions

Nanocomposite materials of 4 nm oleic acid-capped CQD and CoP were prepared and their photophysics is thoroughly investigated. A strong complexation between CQD and CoP is revealed by a development of new absorption band in the Soret band region of CoP. An unprecedented complex formation with binding of the CoP carboxylic anchor to the CQD and coordination between the central metal of the CoP to Te atom on CQD surface are proposed. The favorable lateral binding geometry in CQD/CoP complex is found through computational modeling and it agrees with all the experimental observations. The measured cyclic voltammetry data show the feasibility of ET from CQD to CoP. The first signature of ET from CQD to CoP is the strong luminescence quenching of CQD on nanocomposite material formation. Femtosecond TA spectroscopy proved the ET process in this CQD/CoP nanocomposite material by shortening the CQD excited state lifetime in presence of CoP compared to pure QDs, and a new band formation at the shifted Soret band position. From the global fitting of TA data, the estimated electron transfer time constant from the excited CQD to per CoP molecule is ca. 72 ps and the charge recombination time is $\gg$5 ns where

lateral binding helps to get long-lived charge separation. The ET to CoP activates it as a catalyst for e.g. CO_2 reduction, and the long lifetime of the charge-separated state suggests that CQD/CoP nanocomposites can be a promising material for photocatalytic applications.

Acknowledgement

This project is supported by Jane & Aatos Erkko foundation (JAES/LACOR-31228007701). The authors thank Dr. Alexander Efimov and Dr. Ajayakumar Murugan Rathamony for the valuable discussions. Computational resources were provided by the CSC-IT Center of Science, Espoo, Finland.

Supporting Information Available

Stern–Volmer plot, absorbance spectra of CQD/CoP, Te-TOP/CoP and CQD/CoP1 nanocomposite, Electrochemical measurement, TA spectra, and their fitting. Further computational details and the binding energies for the carboxylic acid model are provided in ESI. ESI is available online free of charge..

References

(1) Jackson, R. B.; Friedlingstein, P.; Andrew, R. M.; Canadell, J. G.; Le, C. Q.; Peters, G. P. Persistent fossil fuel growth threatens the Paris Agreement and planetary health. *Environ. Res. Lett.* **2019**, *14*, 121001.

(2) Li, K.; Peng, B.; Peng, T. Recent Advances in Heterogeneous Photocatalytic CO $_2$ Conversion to Solar Fuels. *ACS Catalysis* **2016**, *6*, 7485–7527.

(3) Francke, R.; Schille, B.; Roemelt, M. Homogeneously Catalyzed Electroreduction of

Carbon Dioxide-Methods, Mechanisms, and Catalysts. *Chem. Rev.* **2018**, *118*, 4631–4701.

(4) Costentin, C.; Drouet, S.; Robert, M.; Savéant, J.-M. A Local Proton Source Enhances CO¡sub¿2¡/sub¿ Electroreduction to CO by a Molecular Fe Catalyst. *Science* **2012**, *338*, 90–94.

(5) Dalle, K. E.; Warnan, J.; Leung, J. J.; Reuillard, B.; Karmel, I. S.; Reisner, E. Electro- and Solar-Driven Fuel Synthesis with First Row Transition Metal Complexes. *Chem. Rev.* **2019**, *119*, 2752–2875.

(6) Costentin, C.; Robert, M.; Savéant, J.-M. Current Issues in Molecular Catalysis Illustrated by Iron Porphyrins as Catalysts of the CO2-to-CO Electrochemical Conversion. *Acc. Chem. Res.* **2015**, *48*, 2996–3006, PMID: 26559053.

(7) Arcudi, F.; Dordević, L.; Nagasing, B.; Stupp, S. I.; Weiss, E. A. Quantum Dot-Sensitized Photoreduction of CO_2 in Water with Turnover Number > 80,000. *J. Am. Chem. Soc.* **2021**, *143*, 18131–18138, PMID: 34664969.

(8) Shen, J.; Kortlever, R.; Kas, R.; Birdja, Y. Y.; Diaz-Morales, O.; Kwon, Y.; Ledezma-Yanez, I.; Schouten, K. J. P.; Mul, G.; Koper, M. T. M. Electrocatalytic reduction of carbon dioxide to carbon monoxide and methane at an immobilized cobalt protoporphyrin. *Nature Comm.* **2015**, *6*, 8177.

(9) Lian, S.; Kodaimati, M. S.; Dolzhnikov, D. S.; Calzada, R.; Weiss, E. A. Powering a CO $_2$ Reduction Catalyst with Visible Light through Multiple Sub-picosecond Electron Transfers from a Quantum Dot. *J. Am. Chem. Soc.* **2017**, *139*, 8931–8938.

(10) Chen, Z.; Hu, Y.; Wang, J.; Shen, Q.; Zhang, Y.; Ding, C.; Bai, Y.; Jiang, G.; Li, Z.; Gaponik, N. Boosting Photocatalytic CO2 Reduction on CsPbBr3 Perovskite Nanocrystals by Immobilizing Metal Complexes. *Chem. Mater.* **2020**, *32*, 1517–1525.

(11) Kamat, P. V. Boosting the Efficiency of Quantum Dot Sensitized Solar Cells through Modulation of Interfacial Charge Transfer. *Acc. Chem. Res.* **2012**, *45*, 1906–1915.

(12) Franceschetti, A.; Zhang, Y. Multiexciton Absorption and Multiple Exciton Generation in CdSe Quantum Dots. *Phys. Rev. Lett.* **2008**, *100*, 136805.

(13) Konstantatos, G., Sargent, E. H., Eds. *Colloidal Quantum Dot Optoelectronics and Photovoltaics*; Cambridge University Press, 2013.

(14) Pan, Z.; Mora-Seró, I.; Shen, Q.; Zhang, H.; Li, Y.; Zhao, K.; Wang, J.; Zhong, X.; Bisquert, J. High-Efficiency "Green" Quantum Dot Solar Cells. *J. Am. Chem. Soc.* **2014**, *136*, 9203–9210.

(15) Weiss, E. A. Designing the Surfaces of Semiconductor Quantum Dots for Colloidal Photocatalysis. *ACS Energy Lett.* **2017**, *2*, 1005–1013.

(16) Chang, C. M.; Orchard, K. L.; Martindale, B. C. M.; Reisner, E. Ligand removal from CdS quantum dots for enhanced photocatalytic H $_2$ generation in pH neutral water. *J. Mater. Chem. A* **2016**, *4*, 2856–2862.

(17) Wagner, A.; Sahm, C. D.; Reisner, E. Towards molecular understanding of local chemical environment effects in electro- and photocatalytic CO_2 reduction. *Nat Catal* **2020**, *3*, 775–786.

(18) Huang, J.; Huang, Z.; Yang, Y.; Zhu, H.; Lian, T. Multiple Exciton Dissociation in CdSe Quantum Dots by Ultrafast Electron Transfer to Adsorbed Methylene Blue. *J. Am. Chem. Soc.* **2010**, *132*, 4858–4864.

(19) Zhu, H.; Yang, Y.; Wu, K.; Lian, T. Charge Transfer Dynamics from Photoexcited Semiconductor Quantum Dots. *Annu. Rev. Phys. Chem.* **2016**, *67*, 259–281.

(20) Mandal, S.; George, L.; Tkachenko, N. V. Charge transfer dynamics in CsPbBr $_3$ perovskite quantum dots–anthraquinone/fullerene (C $_{60}$) hybrids. *Nanoscale* **2019**, *11*, 862–869.

(21) Kuehnel, M. F.; Orchard, K. L.; Dalle, K. E.; Reisner, E. Selective Photocatalytic CO_2 Reduction in Water through Anchoring of a Molecular Ni Catalyst on CdS Nanocrystals. *J. Am. Chem. Soc.* **2017**, *139*, 7217–7223.

(22) Kambhampati, P. Unraveling the Structure and Dynamics of Excitons in Semiconductor Quantum Dots. *Acc. Chem. Res.* **2011**, *44*, 1–13.

(23) Klimov, V. I. Optical Nonlinearities and Ultrafast Carrier Dynamics in Semiconductor Nanocrystals. *J. Phys. Chem. B* **2000**, *104*, 6112–6123.

(24) Grimaldi, G.; Geuchies, J. J.; van der Stam, W.; du Fossé, I.; Brynjarsson, B.; Kirkwood, N.; Kinge, S.; Siebbeles, L. D.; Houtepen, A. J. Spectroscopic Evidence for the Contribution of Holes to the Bleach of Cd-Chalcogenide Quantum Dots. *Nano Lett.* **2019**, *19*, 3002–3010.

(25) Kambhampati, P. Hot Exciton Relaxation Dynamics in Semiconductor Quantum Dots: Radiationless Transitions on the Nanoscale. *J. Phys. Chem. C* **2011**, *115*, 22089–22109.

(26) Dana, J.; Haggag, O. S.; Dehnel, J.; Mor, M.; Lifshitz, E.; Ruhman, S. Testing the fate of nascent holes in CdSe nanocrystals with sub-10 fs pump–probe spectroscopy. *Nanoscale* **2021**, *13*, 1982–1987.

(27) Kang, S.; Yasuda, M.; Miyasaka, H.; Hayashi, H.; Kawasaki, M.; Umeyama, T.; Matano, Y.; Yoshida, K.; Isoda, S.; Imahori, H. Light Harvesting and Energy Transfer in Multiporphyrin-Modified CdSe Nanoparticles. *Chem Sus Chem* **2008**, *1*, 254–261.

(28) Zhu, H.; Song, N.; Lian, T. Wave Function Engineering for Ultrafast Charge Separation

and Slow Charge Recombination in Type II Core/Shell Quantum Dots. *J. Am. Chem. Soc.* **2011**, *133*, 8762–8771.

(29) Mandal, H.; Chakali, M.; Venkatesan, M.; Bangal, P. R. Hot Electron Transfer from CdTe Quantum Dot (QD) to Porphyrin and Ultrafast Electron Transfer from Porphyrin to CdTe QD in CdTe QD–Tetrakis(4-carboxyphenyl)porphyrin Nanocomposites. *J. Phys. Chem. C* **2021**, *125*, 4750–4763.

(30) Keane, P. M.; Gallagher, S. A.; Magno, L. M.; Leising, M. J.; Clark, I. P.; Greetham, G. M.; Towrie, M.; Gun'ko, Y. K.; Kelly, J. M.; Quinn, S. J. Photophysical studies of CdTe quantum dots in the presence of a zinc cationic porphyrin. *Dalton Trans.* **2012**, *41*, 13159.

(31) Hart, A. S.; Kc, C. B.; Gobeze, H. B.; Sequeira, L. R.; D'Souza, F. Porphyrin-Sensitized Solar Cells: Effect of Carboxyl Anchor Group Orientation on the Cell Performance. *ACS Appl. Mater. Interfaces* **2013**, *5*, 5314–5323.

(32) Liao, M.-S.; Scheiner, S. Electronic structure and bonding in metal porphyrins, metal=Fe, Co, Ni, Cu, Zn. *J. Chem Phys* **2002**, *117*, 205–219.

(33) Aly, S. M.; Ahmed, G. H.; Shaheen, B. S.; Sun, J.; Mohammed, O. F. Molecular-structure Control of Ultrafast Electron Injection at Cationic Porphyrin–CdTe Quantum Dot Interfaces. *J. Phys. Chem. Lett.* **2015**, *6*, 791–795.

(34) Lian, S.; Kodaimati, M. S.; Weiss, E. A. Photocatalytically Active Superstructures of Quantum Dots and Iron Porphyrins for Reduction of CO_2 to CO in Water. *ACS Nano* **2018**, *12*, 568–575.

(35) Bonin, J.; Maurin, A.; Robert, M. Molecular catalysis of the electrochemical and photochemical reduction of CO_2 with Fe and Co metal based complexes. Recent advances. *Coord. Chem. Rev.* **2017**, *334*, 184–198.

(36) Peng, Z. A.; Peng, X. Formation of High-Quality CdTe, CdSe, and CdS Nanocrystals Using CdO as Precursor. *J. Am. Chem. Soc.* **2001**, *123*, 183–184.

(37) Paolesse, R.; Monti, D.; La Monica, L.; Venanzi, M.; Froiio, A.; Nardis, S.; Di Natale, C.; Martinelli, E.; D'Amico, A. Preparation and Self-assembly of Chiral Porphyrin Diads on the Gold Electrodes of Quartz Crystal Microbalances: A Novel Potential Approach to the Development of Enantioselective Chemical Sensors. *Eur. J. Chem.* **2002**, *8*, 2476.

(38) Enkovaara, J.; Rostgaard, C.; Mortensen, J.; Chen, J.; Dułak, M.; Ferrighi, L.; Gavnholt, J.; Glinsvad, C.; Haikola, V.; Hansen, H., et al. Electronic structure calculations with GPAW: a real-space implementation of the projector augmented-wave method. *J. Phys.: Condensed Matter* **2010**, *22*, 253202–253225.

(39) Perdew, J. P.; Burke, K.; Ernzerhof, M. Generalized gradient approximation made simple. *Phys. Rev. Lett.* **1996**, *77*, 3865.

(40) Caldeweyher, E.; Bannwarth, C.; Grimme, S. Extension of the D3 Dispersion Coefficient Model. *J. Chem. Phys.* **2017**, *147*, 034112.

(41) Yu, W. W.; Qu, L.; Guo, W.; Peng, X. Experimental Determination of the Extinction Coefficient of CdTe, CdSe, and CdS Nanocrystals. *Chem. Mater.* **2003**, *15*, 2854–2860.

(42) Song, N.; Zhu, H.; Jin, S.; Zhan, W.; Lian, T. Poisson-Distributed Electron-Transfer Dynamics from Single Quantum Dots to C60 Molecules. *ACS Nano* **2011**, *5*, 613–621.

(43) Kamal, J. S.; Omari, A.; Van Hoecke, K.; Zhao, Q.; Vantomme, A.; Vanhaecke, F.; Capek, R. K.; Hens, Z. Size-Dependent Optical Properties of Zinc Blende Cadmium Telluride Quantum Dots. *J. Phys. Chem. C* **2012**, *116*, 5049–5054.

(44) Haddad, R. E.; Gazeau, S.; Pécaut, J.; Marchon, J.-C.; Medforth, C. J.; Shelnutt, J. A.

Origin of the Red Shifts in the Optical Absorption Bands of Nonplanar Tetraalkylporphyrins. *J. Am. Chem. Soc.* **2003**, *125*, 1253–1268.

(45) Ryeng, H.; Ghosh, A. Do Nonplanar Distortions of Porphyrins Bring about Strongly Red-Shifted Electronic Spectra? Controversy, Consensus, New Developments, and Relevance to Chelatases. *Journal of the American Chemical Society* **2002**, *124*, 8099–8103, PMID: 12095355.

(46) Shah, S. H.; Azam, A.; Rafiq, M. A. Atomistic Simulations of CdS Morphologies. *Cryst. Growth. Des.* **2015**, *15*, 1792.

(47) Wu, K.; Li, Q.; Du, Y.; Chen, Z.; Lian, T. Ultrafast exciton quenching by energy and electron transfer in colloidal CdSe nanosheet–Pt heterostructures. *Chem. Sci.* **2015**, *6*, 1049–1054.

(48) Jin, S.; Son, H.-J.; Farha, O. K.; Wiederrecht, G. P.; Hupp, J. T. Energy Transfer from Quantum Dots to Metal–Organic Frameworks for Enhanced Light Harvesting. *J. Am. Chem. Soc.* **2013**, *135*, 955–958.

(49) Ray, A.; Bauri, A.; Bhattacharya, S. Study of chemical physics on energy transfer phenomenon between quantum dots and a designed diporphyrin in solution. *J. Mol. Liq.* **2018**, *263*, 64–71.

(50) Yu, H.; Baskin, J.; Steiger, B.; Wan, C.; Anson, F.; Zewail, A. Femtosecond dynamics of metalloporphyrins: electron transfer and energy redistribution. *Chem. Phys. Lett* **1998**, *293*, 1–8.

(51) Yu, H.-Z.; Baskin, J. S.; Steiger, B.; Anson, F. C.; Zewail, A. H. Femtosecond Dynamics and Electrocatalysis of the Reduction of O_2: Tetraruthenated Cobalt Porphyrins. *J. Amer. Chem. Soc.* **1999**, *121*, 484–485.

(52) Dana, J.; Maity, P.; Ghosh, H. N. Hot-electron transfer from the semiconductor domain to the metal domain in CdSe@CdSAu nano-heterostructures. *Nanoscale* **2017**, *9*, 9723–9731.

(53) Ghosh, T.; Dehnel, J.; Fabian, M.; Lifshitz, E.; Baer, R.; Ruhman, S. Spin Blockades to Relaxation of Hot Multiexcitons in Nanocrystals. *J. Phys. Chem. Lett.* **2019**, *10*, 2341–2348.

(54) Tkachenko, N. V. Effect of the Donor/Acceptor Size on the Rate of Photo-Induced Electron Transfer. *Photochem* **2022**, *2*, 918–931.

(55) Peterson, M. D.; Jensen, S. C.; Weinberg, D. J.; Weiss, E. A. Mechanisms for Adsorption of Methyl Viologen on CdS Quantum Dots. *ACS Nano* **2014**, *8*, 2826–2837.

(56) Padgaonkar, S.; Amsterdam, S. H.; Bergeron, H.; Su, K.; Marks, T. J.; Hersam, M. C.; Weiss, E. A. Molecular-Orientation-Dependent Interfacial Charge Transfer in Phthalocyanine/MoS_2 Mixed-Dimensional Heterojunctions. *J. Phys. Chem. C* **2019**, *123*, 13337–13343.

TOC Graphic

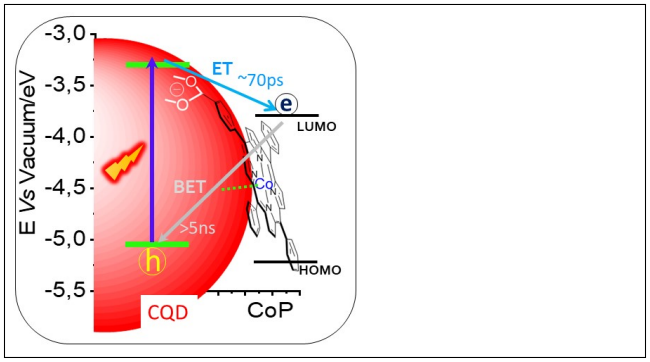
-3,0
-3,5
-4,0
-4,5
-5,0
-5,5
E Vs Vacuum/eV
ET ~70ps
e
LUMO
BET
>5ns
h
HOMO
CQD
CoP